

The Astrochemistry Low-energy Electron Cross-Section (ALeCS) database I.

Semi-empirical electron-impact ionization cross-section calculations and ionization rates

Brandt A. L. Gaches^{1,2*}, Tommaso Grassi³, Stefan Vogt-Geisse⁴, Giulia M. Bovolenta⁴, Claire Vallance⁵, David Heathcote⁵, Marco Padovani⁶, Stefano Bovino^{7,8,9}, and Prasanta Gorai^{1,10}

¹ Department of Space, Earth and Environment, Chalmers University of Technology, Gothenburg SE-412 96, Sweden

² Center of Planetary Systems Habitability, The University of Texas at Austin, USA

³ Max Planck Institute for Extraterrestrial Physics, Giessenbachstrasse 1, 85748 Garching bei München, Germany

⁴ Departamento de Físico-Química, Facultad de Ciencias Químicas, Universidad de Concepción, Concepción, Chile

⁵ Department of Chemistry, University of Oxford, Chemistry Research Laboratory, 12 Mansfield Road, Oxford OX1 3TA, U.K

⁶ INAF–Osservatorio Astrofisico di Arcetri, Largo E. Fermi 5, 50125 Firenze, Italy

⁷ Departamento de Astronomía, Facultad Ciencias Físicas y Matemáticas, Universidad de Concepción Av. Esteban Iturra s/n Barrio Universitario, Casilla 160, Concepción, Chile

⁸ INAF—Istituto di Radioastronomia, Via Gobetti 101, I-40129 Bologna, Italy

⁹ Chemistry Department, Sapienza University of Rome, Ple A. Moro, 00185 Rome, Italy

¹⁰ Department of Chemistry and Molecular Biology, University of Gothenburg, 41296 Gothenburg, Sweden

Accepted XXX. Received YYY; in original form ZZZ

ABSTRACT

Context. Electron-molecule interaction is a fundamental process in radiation-driven chemistry in space, from the interstellar medium to comets. Therefore, knowledge of interaction cross-sections is key. There have been a plethora of both theoretical and experimental studies of total ionization cross-sections spanning from diatomics to complex organics. However, data is often spread over many sources, or not public or readily available.

Aims. We introduce the Astrochemistry Low-energy Electron Cross-Section (ALeCS) database, a public database for electron interaction cross-sections and ionization rates for molecules of astrochemical interest. In particular, in this work, we present the first data release comprising total ionization cross-sections and ionization rates for over 200 neutral molecules.

Methods. We include optimized geometries and molecular orbital energies at various levels of quantum chemistry theory. Further, for a subset of the molecules we have calculated ionization potentials. We compute total ionization cross-sections using the binary-encounter Bethe model and screening-corrected additivity rule, and ionization rates and reaction network coefficients for molecular cloud environments.

Results. We present the cross-sections and reaction rates for >200 neutral molecules ranging from diatomics to complex organics, with the largest being C₁₄H₁₀. We find that the screening-corrected additivity rule cross-sections generally significantly overestimate experimental total ionization cross-sections. We demonstrate that our binary-encounter Bethe cross-sections agree well with experimental data. We show that the ionization rates scale roughly linearly with the number of constituent atoms in the molecule.

Conclusions. We introduce and describe the public ALeCS database. For the initial release, we include total ionization cross-sections for >200 neutral molecules and several cations and anions calculated with different levels of quantum chemistry theory, the chemical reaction rates for the ionization, and network files in the formats of the two most popular astrochemical networks, the Kinetic Database for Astrochemistry and UMIST. The database will be continuously updated for more molecules and interactions.

Key words. Astrochemistry - Molecular data - Molecular processes - ISM: molecules - ISM: cosmic rays

1. Introduction

Observational studies of molecular gas within the Milky Way have revealed a diverse zoo of about 300 molecules, from simple diatomics such as H₂ and CO, to ever more complex molecules, such as NC₄NH⁺ (Agúndez et al. 2023), NH₂C(O)CH₂OH (syn-glycolamide, Rivilla et al. 2023), 2-C₉H₇CN (2-Cyanoindene, Sita et al. 2022), and H₂CCCHC₃N (cyanoacetyleneallene, Shingledecker et al. 2021). Due to the cold temperatures of the interstellar medium (~10-50 K), much of the gas-phase chem-

istry is driven through ion-neutral initiated chemistry (Larsson et al. 2012; Tielens 2013; van Dishoeck 2014). In regions shielded from external radiation, highly energetic charged particles, known as cosmic rays, in particular protons and secondary electrons, and photons, provide the primary ionization source (Umebayashi & Nakano 1981). Finally, chemical models of ices irradiated by energetic particles or X-ray radiation, such as interstellar dust grains and comets, necessarily need to include electron-impact ionization cross-sections for as many molecules as possible in order to account for electron production and subsequent interactions (e.g. Shingledecker et al. 2020).

* E-mail: brandt.gaches@chalmers.se

Astrochemical models describe the evolution of vast chemical networks over time for a wide range of physical environments, including the effects of gas density, temperature, atomic abundances, and radiation environments. There are two key astrochemical databases containing the required reaction rate coefficients, KIDA¹ (Wakelam et al. 2012) and UMIST² (McElroy et al. 2013). However, for cosmic-ray ionization, there is a substantial paucity in reaction rate data, with KIDA and UMIST combined only reporting reaction rate coefficients for H, He, C, O, N, H₂, N₂, and CO. In astrochemical models, these reaction rates are expressed in the form

$$\zeta_{m,T} = c_{m,T} \zeta_{\text{H}_2,T}, \quad (1)$$

where c_m is a scaling factor that relates the rate of the reaction of interest to the total ionization rate, $\zeta_{\text{H}_2,T}$, of H₂. The coefficients are computed with respect to some reference total H₂ ionization rate, typically $\zeta_{\text{H}_2,0} \approx 3 \times 10^{-17} \text{ s}^{-1}$, often referred to as the “canonical” or “fiducial” ionization rate.

The coefficients $c_{m,T}$ in KIDA and UMIST date back to early studies from the 1970s and 1980s (Cravens et al. 1975; Cravens & Dalgarno 1978; Glassgold & Langer 1974; Black 1975). For molecules containing atoms beyond hydrogen and helium, computed ionization rates often scaling relationships between the high-energy cross-sections of the molecules, and assumed a Voyager-like proton cosmic-ray spectrum. However, there has been substantial development in the theoretical calculation and experimental measurements of these cross-sections. Further, it has been demonstrated that the spectrum of secondary non-thermal electrons is highly sensitive to the local proton cosmic-ray spectral shape (Ivlev et al. 2021). Observations of the ionization rate have demonstrated that the H₂ ionization rate within molecular clouds is more commonly around 10^{-16} s^{-1} (Caselli et al. 1998; van der Tak & van Dishoeck 2000; Neufeld et al. 2010; Indriolo & McCall 2012; Indriolo et al. 2015; Neufeld & Wolfire 2017; Sabatini et al. 2020; Luo et al. 2023a,b; Sabatini et al. 2023), with trend of decreasing towards increasing column density, consistent with a combination of energy losses and possible diffusive transport (e.g. Padovani et al. 2009, 2018; Silsbee & Ivlev 2019; Phan et al. 2023).

There have now been a sizable number of studies reporting computed values for the total electron-impact ionization cross-sections of a variety of molecules. Public databases such as PlasmaData³ (Zhong et al. 2021), BEAMDB⁴ (Marinković et al. 2017), the US-based National Institute Standards and Technology (NIST) Electron-Impact cross-sections for Ionization and Excitation Database⁵, and the Japanese-based National Institute for Fusion Science (NIFS) database⁶ have compiled the cross-sections for a wide range of molecules, often for use in plasma physics, medicine, or other industry applications. The latter of these databases comprises a significant number of experimental and evaluated ionization cross-sections. Recently Heathcote & Vallance (2018) and Zhou et al. (2019) presented large datasets of calculated and experimental cross-sections, respectively, for a wide range of molecules of astrochemical interest. These datasets and databases represent a significant advancement in the availability of cross-section data for astrochemi-

cal use. However, they generally do not include molecules containing heavier atoms, and also do not report on computed and recommended reaction rate coefficients. Furthermore, databases comprising a large number of ionization cross-sections often either do not use a standard evaluation process or do not provide the data in a readily accessible way.

In this paper, we present a new public database containing electron ionization cross-sections and cosmic-ray ionization rate coefficients for over 200 molecules of astrochemical interest. We report the cross-sections for low-energy electrons ($10 \text{ eV} \leq E_e \leq 5000 \text{ eV}$) for each of these molecules using both a screening-corrected additivity rule and the binary-encounter Bethe model cross-section, the molecular orbital binding and kinetic energies utilized, and recommended total reaction rate coefficients for molecular cloud environments. Crucially, the cross-sections and coefficients are evaluated for nearly all molecules using the same procedure, providing homogeneous datasets to enable better comparisons and consistency.

2. Methods

We present here the methods for the different approaches of calculating the total electron-impact ionization cross sections, then quantum chemistry computations performed, and the calculations of the resulting ionization rates. In brief, we calculate three different models of the electron-impact total ionization rate: the screening-corrected additivity rule (SCAR), binary-encounter Bethe (BEB), and damped-binary-encounter Bethe (dBEB) models. In particular, we explore the accuracy of the SCAR method, since it may become more applicable for larger molecules due to the computational expense required for accurately computing BEB-related cross sections. The latter models require knowledge of the electronic structure, while the former only requires knowledge of the geometry and a basis set of electron-atom ionization cross sections. For our molecule selection, we choose the primary molecules used in astrochemical networks with reaction rate data on the kinetics database KIDA.

2.1. Electron-atom ionization cross-sections

The semi-empirical method we use requires a basis of electron-atom ionization cross-sections. We obtain these cross-sections by fitting a polynomial to experimental data, from the NIFS AMIDIS-ION⁵ database, where the electron-atom ionization cross section takes the form:

$$\sigma_i(E) = \begin{cases} 0 & \text{for } E_e < \text{IP}_i \\ a_0^2 \left(\frac{x-1}{x} \right) \left[c_0^2 \left(\frac{\ln x}{x} \right) + \sum_{k=1}^5 \frac{c_k}{x^k} \right] & \text{for } E_e \geq \text{IP}_i, \end{cases} \quad (2)$$

where a_0 is the Bohr radius, E_e is the electron energy, IP_i is the ionization potential of the atomic species i , $x = E_e/\text{IP}_i$, and c_k are fitting coefficients. Figure 1 shows the experimental data used and the fitted cross-sections. Table 1 shows the results of the fits of Equation 2 for each atom.

2.2. Semi-empirical cross-section calculation

2.2.1. SCAR Method

The cross-sections are computed using the *screening-corrected additivity rule* (SCAR) (Blanco & García 2003; Blanco et al. 2010). This method enables the quick computation of molecular cross-sections using just a pre-computed basis of electron-atom ionization cross-sections. SCAR is an additivity rule which takes

¹ <https://kida.astrochem-tools.org/>

² <http://udfa.ajmarkwick.net/>

³ <http://plasma.mathboylinlin.com/>

⁴ <http://servo.aob.rs/emol/>

⁵ <https://www.nist.gov/pml/electron-impact-cross-sections-ionization-and-excitation-database>

⁶ <https://dbshino.nifs.ac.jp/nifsdb/>

Table 1: Electron-atom ionization cross-section fitted coefficients for Equation 2. Coefficients are given in the form $a(b) = a \times 10^b$.

Atom	c_0	c_1	c_2	c_3	c_4	c_5
H	2.813905(0)	-1.101730(0)	1.838647(1)	-3.577323(1)	2.554819(1)	-2.358867(0)
He	1.313597(0)	1.261778(1)	-5.359803(1)	1.153092(2)	-1.239072(2)	5.145647(1)
C	7.575591(0)	-5.795490(1)	2.264768(2)	-6.500235(2)	9.067897(2)	-4.246887(2)
N	6.180613(0)	-2.659850(1)	6.022187(1)	-1.036028(2)	1.070141(2)	-1.959618(1)
O	5.400010(0)	4.102912(0)	-1.951275(2)	6.362247(2)	-7.754242(2)	3.372681(2)
P	8.463675(0)	3.806864(1)	-3.042532(2)	8.754706(2)	-1.029666(3)	4.429356(2)
S	9.674459(0)	-5.296533(1)	-8.623544(1)	6.587089(2)	-9.794655(2)	4.823979(2)
Ar	6.618024(0)	9.689090(-1)	-1.248942(2)	5.386474(2)	-7.977861(2)	4.114582(2)

into account the effective geometrical overlap of the atomic electron cross-sections. The cross-section for a specific molecule, m , is given by

$$\sigma_{m,\text{SCAR}}(E) = \sum_i s_i \sigma_i(E), \quad (3)$$

where the sum is carried out over all constituent atoms and $\sigma_i(E)$ is the electron-atom ionization cross-section for atom, i . Under the simplest additivity rules, $s_i = 1$. For the SCAR method, the additivity coefficients, s_i , are

$$s_i = \sum_{k=1}^{N_k} \frac{(-1)^{k+1} \varepsilon_i^{(k)}}{k!}, \quad (4)$$

where N_k is the number of perturbation terms included. The coefficients, $\varepsilon_i^{(k)}$, follow the recursive relation

$$\varepsilon_i^{(1)} = 1 \quad (5)$$

$$\varepsilon_i^{(k)} = \frac{N_k - k + 1}{N_k - 1} \sum_{j(\neq i)} \frac{\sigma_j \varepsilon_j^{(k-1)}}{\alpha_{ji}}, \quad k = 2, \dots, N, \quad (6)$$

where $\alpha_{ji} = \max(4\pi r_{ij}^2, \sigma_i, \sigma_j)$, and r_{ij} is the distance between atoms i and j . The terms in Equation 4 amount to higher-order correction factors accounting for the overlap of the cross-sections of all the individual items. Due to the recursive nature of the coefficients (Eq. 5), including higher-order correction terms leads to an exponential increase in computational cost. However, this is alleviated by building a dictionary cache during the recursion to avoid recomputing the same screening terms. This leads to a sub-linear increase in computing time against maximum k -atom screening correction included.

2.2.2. BEB cross-sections

The semi-empirical binary-encounter Bethe (BEB) cross-section was developed as a simplification of the binary-encounter dipole cross-section (Kim & Rudd 1994; Hwang et al. 1996). This cross-section has been found to provide a reasonable match with experimental data, and requires only knowledge of the molecular orbital energies. BEB cross-section are the base of numerous cross-section databases, in particular the NIST database. The BEB cross-section is defined as:

$$\sigma_{m,\text{BEB}} = \sum_{\ell} \left[\frac{S_{\ell}}{t_{\ell} + (u_{\ell} + 1)} \right] \left[\frac{\ln t_{\ell}}{2} \left(1 - \frac{1}{t_{\ell}^2} \right) + \right. \quad (7)$$

$$\left. \left(1 - \frac{1}{t_{\ell}} - \frac{\ln t_{\ell}}{t_{\ell} + 1} \right) \right], \quad (8)$$

where the sum is over orbitals, indexed ℓ , $t_{\ell} = E_e/B_{\ell}$, $u_{\ell} = U_{\ell}/B_{\ell}$ and $S_{\ell} = 4\pi a_0^2 n_{\ell} \left(\frac{R_{\infty}}{B_{\ell}} \right)^2$. Here, B_{ℓ} and U_{ℓ} are the orbital binding and orbital kinetic energies of the ejected electron, respectively, n_{ℓ} is the orbital occupation number, and R_{∞} is the Rydberg constant. The parameters B_{ℓ} and U_{ℓ} are generally computed using electronic structure methods.

We also propose a modified version of the BEB cross-section (dBEB) to dampen the impact of orbitals with binding energies greater than the ionization potential. In dBEB cross-section formulation, the B_{ℓ} is scaled by an exponential function such that the modified binding energy of orbital ℓ is given by:

$$B'_{\ell} = B_{\ell} e^{-(1-B_{\ell}/\text{IP})}, \quad (9)$$

As we demonstrate below, this prevents the BEB cross-section from over-estimating with respect to experimental values, which are generally upper limits. In general, BEB cross sections under-predict experimental results at higher energies since they only account for single ionizations, while experimental data, where the measured signal is generally the ion current, includes contributions from multiple ionization events which contribute more to the measured signal per event than single ionizations.

2.3. Quantum chemistry computations

We selected a set of 156 neutral species including atoms and molecules, for the calculation of BEB and dBEB cross-sections. The initial structures are taken from NIST Computational Chemistry Comparison and Benchmark DataBase⁷ (CC-CBDB) database (Johnson 2022). The equilibrium geometries were obtained at MP2/aug-cc-pVTZ method and basis set. To validate the accuracy of this level of theory we also optimized a group of 50 structures using the highly accurate DF-CCSD(T)-F12/cc-pVQZ-F12 (U-CCSD(T)-F12/cc-pVQZ-F12 for radical species). The set of electron binding energy (eBE), B_{ℓ} , taken as the negative of the energy of orbital ℓ , is computed by means of electron propagator theory (EPT) in its P3+ implementation along with aug-cc-pVTZ basis. In EPT, electron correlation is taken into account, thus providing a more accurate value for B_{ℓ} , compared to Hartree-Fock (HF) canonical orbital energies. For the computation of the BEB cross-sections, we use the EPT-corrected orbital energies if the related pole strength is greater than 0.8, or else we use the HF canonical orbital energies as an estimate of the B_{ℓ} . Since the lowest B_{ℓ} – namely the IP, according to Koopmans’ theorem – is the predominant contribution to the BEB cross-section, the accuracy of the eBE plays a significant role.

⁷ <https://cccbdb.nist.gov/>

We computed vertical IPs for 148 molecules in our sample, using the Density Functional Theory (DFT) method CAM-B3LYP/aug-cc-pVQZ, employing the D3 empirical dispersion. Furthermore, to validate the accuracy of the IPs we compare the DFT results to highly accurate values that we computed at CCSD(T) paired with complete basis set (CBS) extrapolation using cc-pVXZ (X=D,T) basis functions, for a subset of 56 species. This subset consists of molecules with 2-4 atoms.

Computations were performed using software packages **GAUSSIAN16**⁸ (Frisch et al. 2016), **MOLPRO**⁹ (Werner et al. 2012, 2020), and **Psi4**¹⁰ (Smith et al. 2020b, interfaced with the **QCFRACTAL**¹¹ infrastructure, see Smith et al. 2020a). Details of the different electronic structure methods are presented in Table 2.

Finally, we include molecular geometries and orbitals from **Heathcote & Vallance** (2018), which comprises 141 molecules including 6 anions and 18 cations. These were computed at the HF/aug-cc-pVTZ level, with a small subset at the MP2/aug-cc-pVTZ level (C₄H, C₅H, C₅N, and C₆H, see **Heathcote & Vallance** 2018 for details). H₂ is computed at the CCSD(T)/aug-cc-pVTZ level. We also include the non-published calculated data for cations and anions which were previously excluded since there is a lack of experimental data for these molecules to benchmark against, and so the method of calculation could not be confirmed. As such, we exclude the anions and cations from the reaction rate plots, although they are included in the full database.

2.4. Low-energy electron spectrum and ionization rate

Low-energy electrons in molecular clouds are primarily generated as secondary particles produced by ionization of H₂ by primary cosmic-ray protons or electrons. We obtain depth-dependent electron spectra, e.g., $j_e(E_e, N_{\text{H}_2})$ where N_{H_2} is the H₂ column density in the cloud following the new rigorous prescription in Ivlev et al. (2021), with corrections for H₂-excitation and new H₂-electron cross-sections (Padovani et al. 2022).

The depth-dependent electron ionization rate of a molecule, m , is given by adding the contributions of primary protons, $\zeta_{p,m}(N_{\text{H}_2})$, using the approximation $m_e E_p \approx m_p E_e$,

$$\zeta_{p,m}(N_{\text{H}_2}) = 2\pi \int j_p(E_p, N_{\text{H}_2}) \sigma_m \left[(m_e/m_p) E_p \right] dE_p, \quad (10)$$

primary electrons,

$$\zeta_{e,m}(N_{\text{H}_2}) = 2\pi \int j_e(E_e, N_{\text{H}_2}) \sigma_m(E_e) dE_e, \quad (11)$$

and secondary electrons from both primary protons and electrons

$$\zeta_{se,m}(N_{\text{H}_2}) = 4\pi \int j_{se}(E_e, N_{\text{H}_2}) \sigma_m(E_e) dE_e, \quad (12)$$

where se represents secondary electrons. The factors of 2π and 4π account for fluxes which are assumed to be plane parallel and isotropic, respectively. The total ionization rate for a molecule is then, $\zeta_m = \zeta_{p,m} + \zeta_{e,m} + \zeta_{se,m}$. The factor of 4π comes from treating the secondary electrons as an isotropic local source.

We use the “High” primary proton and proton-induced secondary electron spectra as a function of column density from

Padovani et al. (2022), who computed the electron spectrum down to 1 eV following the recent more rigorous theory of Ivlev et al. (2021). The High proton spectrum has been calibrated to match diffuse gas observations of the H₂ ionization rate, which are not reproduced with a Voyager-like spectrum (Ivlev et al. 2015; Padovani et al. 2018). We also use an interstellar primary electron spectrum from Padovani et al. (2018), and their induced secondary electrons. The secondary electron computation assumes that the gas is fully molecular and includes energy losses from Coulomb interactions, as well as for H₂ ionizations and electronic and rovibrational excitations. We define our column-dependent total ionization rate coefficient for species m , $c_{m,T}(N_{\text{H}_2})$ from

$$\zeta_{m,T}(N_{\text{H}_2}) = c_{m,T}(N_{\text{H}_2}) \zeta_{\text{H}_2,T}(N_{\text{H}_2}), \quad (13)$$

where $\zeta_{\text{H}_2,T}(N_{\text{H}_2})$ is the total H₂ ionization rate including all primary, secondary, and tertiary processes. We report the column-density average coefficient, $\bar{c}_{m,T}$, for cloud column density range, $N_{\text{H}_2} \approx 10^{20} - 10^{23} \text{ cm}^{-2}$, although we note that the coefficients only marginally scale with column density. Hereafter, we denote $\bar{c}_{m,T}$ as $c_{m,T}$, due to the marginal scaling with column density. In general, since the BEB cross sections perform better than the SCAR data in comparisons against experimental data, we report here only the coefficients using the BEB cross section, although all cross sections are available in the database.

3. Results

In total, we have computed the structure, orbitals, and cross-sections for 202 unique (by composition, not counting isomers) neutral molecules ranging in size from two to 24 atoms including data augmented by the results from **Heathcote & Vallance** (2018). Figure 2 shows the distribution of the number of atoms for the molecules in our database; while most of the molecules have fewer than six atoms, we include some with up to 24 atoms (C₁₄H₁₀). In cases where KIDA does not specify an isomer, but multiple isomers exist, we take the most stable isomer. We detail below a summary of the results, with all of the data available online in the public database, <https://github.com/AstroBran dt/ALECS>.

3.1. Ionization potentials, electron binding energies, and electron kinetic energies

We present here the ionization potentials computed at both the DFT (CAM-B3LYP) and CCSD(T)/CBS levels, and compare them to the experimental value recommended in NIST. Table 4 shows the resulting ionization potentials in eV for the molecules. Figure 3 shows a comparison between the different calculations and the NIST database. In general, for molecules with fewer than seven atoms, our calculations are consistent with values presented in the NIST database. For molecules with higher ionization potentials, our calculated IPs are generally higher. We find relatively good agreement between the CAM-B3LYP and CCSD(T) calculations, however, there is a general trend that CAM-B3LYP produces smaller IPs compared to CCSD(T) for molecules with IP < 10 eV.

As part of the database, we also present the molecular orbital binding and kinetic energies for each molecule. An example result of this, for CO and H₂O, is presented in Table 5 and Table 6 respectively. The tables show both, the eBEs computed from the canonical HF orbitals and from the EPT theory. The eBE computed with the latter method are smaller than the ones

⁸ <http://gaussian.com/>

⁹ <https://www.molpro.net/>

¹⁰ <https://psicode.org/>

¹¹ <https://github.com/MolSSI/QCFractal>

Table 2: Summary of quantum chemistry methods and citations.

Basis sets	aug-cc-pVXZ (X=T,Q) Complete Basis Set (CBS) extrapolation	Dunning (1989), Dunning T.H. et al. (2001) Helgaker et al. (1997)
Gaussian16	Møller-Plesset second order (MP2)	Møller & Plesset (1934), Frisch et al. (1990a), Frisch et al. (1990b)
	CAM-B3LYP	Becke (1993), Yanai et al. (2004)
	Grimme's dispersion (D3)	Grimme et al. (2010)
	Electron-propagator Theory (EPT), P3+	Migdal & Moszkowski (1968), Ortiz (2005)
Psi4	Coupled Cluster (CCSD(T))	Raghavachari et al. (1989)
MOLPRO	Explicitly correlated Density Fitted CCSD(T) (DF-CCSD(T)-F12)	Györffy & Werner (2018)

obtained with HF since they are corrected to include the instantaneous electron-electron repulsion (electron correlation) in its energy, which increases the energy of the orbitals thus making it easier for an electron to detach. According to Koopmans' theorem, the lowest eBE is equal to the ionization potential of the molecule. Comparing the the values of the EPT-eBE and the IP computed at our best level of theory (CCSD(T)/CBS) excellent agreement can be seen with discrepancies of around 0.2 eV and much improved with respect to HF-eBEs. Given that the lowest eBE carries the most weight in the BEB cross-section, ensuring its accuracy is paramount. Our results not only exhibit a marked improvement over canonical HF values but also suggest that the error related to the electronic structure is minimal. However, for the deep-lying orbitals, no reliable EPR-eBEs can be computed thus we chose to use the HF values for these orbitals.

We find good agreement between our HF-BE data and the NIST electron-impact cross-section database, which uses data from [Hwang et al. \(1996\)](#) computed at the HF/6-311-G level for the eBE. This is expected as the only difference between the NIST and our HF orbital binding energies is a larger atomic orbital basis set in the latter case. However the incorporation of EPT-BE into our database enhances the overall data quality compared to the existing NIST data. We thus conclude that our calculations of orbital binding energies are derived from a robust theoretical framework, offering the required level of accuracy given the underlying assumptions in our cross-section calculations.

Finally, we also include the optimized geometries at the MP2/aug-cc-pVTZ and DF-CCSD(T)-F12/cc-pVDZ-F12 levels presented here and the sample from [Heathcote & Vallance \(2018\)](#) in the database. The geometries are not appreciably different from each other. All geometries were checked that represent minimum energy structures by ensuring that no imaginary frequencies in the diagonalized Hessian matrix is present.

3.2. Low-energy electron cross-sections

As described earlier, we have computed the cross-sections using three different approaches: the screening-corrected additivity rule (SCAR), the binary-encounter Bethe (BEB) model, and the new damped BEB cross-section (dBEB).

The SCAR method is inherently recursive, so care must be taken to avoid exponential increases in computational time with the number of atoms. We utilized recursive caching to speed up the calculations, and only computed to a maximum of the 10-atom screening correction. Figure 4 shows the individual screening corrections, the magnitude of the correction and the total time as a function of the maximum screening terms kept. We find

that the screening terms past the eight-atom screening correction are negligible contributions to the total cross-section, which is dominated by the first few correction factors.

We show results for a subset of the molecules, ranging from simple to complex, to compare the difference between the SCAR and BEB cross-sections. Figure 5 shows these for a subsample of 10 molecules, ranging in size from CO to c-C₆H₆. We find that the SCAR approach generally overestimates the cross-section, although the impact is most pronounced in c-C₆H₆ due to the overlapping of the molecular orbitals. However, given the speed of computing these cross-sections, they may be useful for first investigations if the optimized molecule geometry is known *a priori*.

We perform a closer investigation of the model predictions for a subset of these molecules for which experimental data is available. Figure 7 shows a comparison with experimental data for a subset of molecules, including the simple molecule CO₂, symmetric ring c-C₆H₆, prebiotic species of interest NH₂CHO and carbon chains. Experimental and theoretical cross-section data are known to deviate quite significantly (see discussion in [Zhou et al. 2019](#)). In particular, experimental cross-sections include double ionizations and Auger ionizations, thus overestimating the single ionization cross section. The cross-sections we present here are for single ionization events, with multiple ionizations being left for future work. We find that with our computed data, the BEB slightly overestimates the cross-section at low energy regions while underestimating it in higher energy regions. Nonetheless the values from the BEB calculation are in much better agreement with experimental results than the SCAR or the IAI model. Given that the experimental curve should serve as an upper limit for the theoretical BEB model, and noting that even with highly accurate eBEs it still overestimates the cross-section, we suggest a modified BEB model in which the the contribution from deeper-lying electron ionizations are scaled, to better balance its weight in the total cross-section. As expected, we find that the dBEB corss-section under-predicts the experimental value. Future calculations using the more complicated binary-encounter dipole model ([Kim & Rudd 1994](#)) will be investigated for future releases. In our further analysis, we use the BEB cross sections to calculate the reaction rates, since towards higher energies they tend towards better agreement with data.

3.3. Molecular cloud rate coefficients

We discuss here the molecular cloud reaction rates coefficients, scaled to the total ionization rate (see Section 2.4). Figures 9 - 12 show the coefficients, $c_{m,T}$, for our database sample. There is a

general trend of an increase in $c_{m,T}$ with the size of the molecule. However, for a given number of atoms, there is still substantial scatter due to the geometry and composition. Our reaction rate is marginally less than that reported by UMIST for CO, originally from [Black \(1975\)](#), where they report $c_{CO,T} = 3$ whereas we find $c_{CO,T} = 1.943$. We report the mean coefficients in Table 7, where the mean is taken of the coefficients for total hydrogen nuclei column densities ranging from $10^{20} - 10^{23} \text{ cm}^{-2}$. We note that these reaction rates are tailored for molecular cloud-like environments, e.g. those with a prescribed external cosmic-ray spectrum matching the “High” model from [Padovani et al. \(2022\)](#) (see also [Ilyev et al. 2015](#)), and have total hydrogen nuclei column densities between $10^{20} \leq N_{\text{H}} \leq 10^{23} \text{ cm}^{-2}$.

There is a substantial difference in the reaction rates as found using the SCAR and BEB methods. While the additivity rules account for the *geometric* overlap of the atomic cross-sections, it does not account for the structure of the molecule orbitals nor differences in eBEs due to molecular bonds. Therefore, we do not recommend the use of additivity rules to compute the cross-sections for use in astrochemical modeling, unless it is impractical to compute molecular orbitals and use the BEB cross-section.

Figure 8 shows the mean $c_{m,T}$ coefficient as a function of the number of atoms. Similar to Figure 6, we find a general increase in the reaction rate with the number of constituent atoms. The figure also shows a best-fit relation

$$c_{m,T} = 1.19N_{\text{atom}} + 1.84, \quad (14)$$

where N_{atom} is the number of constituent atoms. The relationship reproduces the general trend for $N_{\text{atom}} \leq 20$. We also fit the coefficients as a function of the number of valence electrons, which produces a slightly better fit

$$c_{m,T} = 0.45N_{\text{v,elec}} - 0.64, \quad (15)$$

where $N_{\text{v,elec}}$ is the number of valence electrons in the molecule. This fit was constrained only for molecules with $9 \leq N_{\text{v,elec}} \leq 70$. In both cases, there is significant scatter of approximately a factor of 2 around the fit trends, so caution should be used if using these for molecules not in the database.

3.4. Database description and file format

We include a number of different formatted files for the total electron-impact cross sections, ionization potentials, molecular and atomic orbitals, and reaction rate coefficients. Cross sections are found in the `ion_xs/` directories for the SCAR, HF, MP2 and CCSD(T) calculations and atoms. Cross-section files are formatted as in the following example, `co_xs`

```
# CO cross section
256
1.00000e+01  0.00000e+00  0.00000e+00
1.04618e+01  0.00000e+00  0.00000e+00
1.09450e+01  0.00000e+00  0.00000e+00
1.14505e+01  0.00000e+00  0.00000e+00
1.19793e+01  0.00000e+00  0.00000e+00
1.25325e+01  0.00000e+00  0.00000e+00
1.31113e+01  0.00000e+00  0.00000e+00
1.37169e+01  0.00000e+00  0.00000e+00
                           {more data}
9.13659e+05  8.52230e-03  6.30487e-03
9.55855e+05  8.17497e-03  6.04801e-03
1.00000e+06  7.84171e-03  5.80155e-03
```

where the first row gives the number of electron energy bins. The later rows give the data in (two) three columns. For BEB cross

sections, the columns provide electron impact energy (eV), BEB cross-section in units of σ_0^2 and, if available, the damped-BEB cross-section in units of σ_0^2 . For SCAR cross sections, the three columns provide energy (eV) and SCAR cross section in units of σ_0^2 .

The orbital information is stored in two directories containing the orbitals in the NIST format, `NIST_orbitals/` and including all orbitals, `full_orbitals/`. An example of the NIST formatted file, `co.norb`

```
#CO NIST Orbitals
#Orbital      B          U          N  Q
1            562.416986  794.326705  2  1
2            309.246847  436.294142  2  1
3            41.332626   78.262641   2  1
4            21.888866   71.857734   2  1
5            17.015000   53.945104   2  1
6            17.015000   53.945104   2  1
7            14.266000   42.788163   2  1
```

where the B column gives the eBE (eV), U gives the average electron kinetic energy (eV), N gives the orbital occupation number and Q is a scaling factor to include higher-order ionization effects. We also show an example of the full orbital file, `co.forb`

```
#CO Full Orbitals
#Alpha orbitals
#Orb.          KE          BE-HF        BE-P3+      Pole
1            794.32671   562.41699    ***       ***
2            436.29414   309.24685    ***       ***
3            78.26264    41.33263    ***       ***
4            71.85773    21.88887    ***       ***
5            53.94510    17.35920    17.015     0.903
6            53.94510    17.35920    17.015     0.903
7            42.78816    15.11922    14.266     0.910
```

where the file will give the information for both alpha and beta orbitals, for open-shell molecules that were computed with an unrestricted formalism. The KE and BE-HF columns give the average electron kinetic energy and eBE (eV) computed by the population analysis in GAUSSIAN16 following geometry optimization. The latter 2 columns include the results from EPT, where *** denotes orbitals where EPT was not computed. For orbitals where it was computed, we include the EPT-corrected HF canonical orbital energies (at P3+ level) results and the pole strength (PS).

We include the computed ionization potentials in the `ips/` directory for the compiled NIST and computed CAM-B3LPY and CCSD(T) molecules. These are two-column files with the molecule and ionization potential in eV. We also include two network files containing all the new molecular and atomic ionization rate coefficients in the `networks/` directory. These network files are in the KIDA and UMIST formats, `alecs.kida.in` and `alecs.umist.d`, respectively. We recommend users to only include ionization rates for molecules in which there are associated recombination rates for the ion. Finally, in the `geoms/` folder we include all molecule geometries computed at the HF, MP2, and CCSD(T) levels. The MP2 and CCSD(T) geometries are formatted as PDB files and the HF geometries as XYZ.

3.5. Astrochemical Modeling

We include the new calculations in a model that uses the KIDA reactions framework, providing a zero-dimensional model as in Sect. 3.1 of [Wakelam et al. \(2015\)](#). It is important to note that, within our context, this test has not been designed to quantify the impact of the new rates in an astrophysical environment, but

to show how the new rate equations are compatible with previously established formats. Therefore, the cross sections may play a more important role in, e.g., ice chemistry, disks, planetary atmospheres, exomoons, or cometary environments. However, this analysis is beyond the aims of the present paper, and it will be discussed in a forthcoming work.

We model a gas with total hydrogen density $n_{\text{H,tot}} = 2 \times 10^4 \text{ cm}^{-3}$, gas temperature $T = 10 \text{ K}$, initial conditions as in Tab. 8, and no dust (e.g., see [Hincelin et al. 2011](#); [Loison et al. 2014](#)). We compute the ionization rate $\zeta(N_{\text{H}_2})$ including protons, primary and secondary electrons, and secondary from primary electrons. Note that the ionization rate is a function of the column density N (see Eq. 13), and that we assume that the visual extinction (necessary for the photochemistry) is $A_V = 1.0638 \times 10^{-21} N$, where N is in units of cm^{-2} . To model the time-dependent evolution of the chemical abundances for 10 Myr, we make use of **KMARX** (Grassi in prep., commit 58f6ac9), a Python-based database that allows us to solve the chemical ordinary differential equations with a standard BDF solver¹² ([Hindmarsh 1983](#)). We include the HTML output produced by the code in the database as a zip file in the `chem_models/` folder, where the reactions present in this work are listed under the class `CRReactionAdv`.

When using our chemical network, we replace the ionization reactions from KIDA where possible (i.e., H, He, N, O, H_2 , and CO) and add the missing ionization rates that will impact the molecules listed in Tab. 8. We do not add the species that creates sinks or sources in the chemical network, i.e., species that only appear in the products or in the reactants, respectively. We also note that, for the sake of comparison, the cosmic-ray reaction rates from KIDA are scaled so that the H_2 ionization matches the ionization rate of molecular hydrogen in our database. The aim of this scaling is to avoid discrepancies determined by different assumptions in the cosmic-ray spectra employed.

Fig. 13 shows the results obtained with the KIDA database reaction rates (solid lines) and calculated with the rates present in this work (dashed lines). For the sake of clarity, we only plot the species that show a difference larger than a tenth of an order of magnitude and reach at least $n(t) = 10^{-8} n_{\text{H,tot}}$ during their evolution. Only a few species present a negligible discrepancy between the two databases. The extent of these variations is minimal because the critical cosmic-ray-driven reactions are very similar in ALeCS and in KIDA, but the results might be less interchangeable in different environments. Also, note that we have assumed that the constituents of the spectra are matching, i.e., both include protons, electrons, and secondary processes, hence the scaling mentioned above.

4. Conclusions

We present the initial data release for the Astrochemistry Low-energy electron cross-section (ALeCS) database. In this release, we include the total ionization cross-sections and ionization rate coefficients for over 200 neutral molecules of astrochemical interest calculated using three different semi-empirical methods: the SCAR ([Blanco & García 2003](#); [Blanco et al. 2010](#)), the BEB model ([Kim & Rudd 1994](#); [Hwang et al. 1996](#)) and a new damped-BEB model (dBEB) presented here. The latter of these dampens orbitals deep within the potential well and was demonstrated to help prevent the BEB model from overestimating the ionization cross-section when compared with experimental results. We also present the ionization rate coefficients, and

molecular ionization rates scaled to a reference total H_2 ionization rate.

The database is fully public, and will include the ionization data described above, along with the molecule orbitals and optimized geometries. In this current release, we only include the semi-empirical ionization cross-sections and reference experimental data. Future releases will include more sophisticated ionization cross-section calculations along with excitation and momentum transfer. Finally, the database will include open-source software tools necessary to couple these processes to astrochemical codes.

Acknowledgements. The MP2 and DFT calculations presented here were performed on the VERA computing cluster, managed by the Chalmers Center for Computational Science and Engineering. BALG and PG are supported by the Chalmers Initiative on Cosmic Origins as Cosmic Origins Postdoctoral Fellows. S.B. is financially supported by ANID Fondecyt Regular (project #1220033), and the ANID BASAL projects ACE210002 and FB210003. CV and DH would like to thank the UK Engineering and Physical Sciences Research Council for funding via Programme Grants EP/V026690/1 and EP/T021675/1. SVG is financially supported by VRID project 2022000507INV. GMB gratefully acknowledges support by ANID Beca de Doctorado Nacional 21200180.

References

- Agúndez, M., Cabezas, C., Marcelino, N., et al. 2023, *A&A*, 669, L1
- Becke, A. D. 1993, *The Journal of Chemical Physics*, 98, 5648
- Black, J. H. 1975, PhD thesis, Harvard University, Massachusetts
- Blanco, F. & García, G. 2003, *Physics Letters A*, 317, 458
- Blanco, F., Rosado, J., Illana, A., & García, G. 2010, *Physics Letters A*, 374, 4420
- Caselli, P., Walmsley, C. M., Terzieva, R., & Herbst, E. 1998, *ApJ*, 499, 234
- Cravens, T. E. & Dalgarno, A. 1978, *ApJ*, 219, 750
- Cravens, T. E., Victor, G. A., & Dalgarno, A. 1975, *Planet. Space Sci.*, 23, 1059
- Dunning, Thom H., J. 1989, *The Journal of Chemical Physics*, 90, 1007
- Dunning T.H., J., Peterson, K. A., & Wilson, A. K. 2001, *Journal of Chemical Physics*, 114, 9244, ISBN: 0021-9606
- Frisch, M. J., Head-Gordon, M., & Pople, J. A. 1990a, *Chemical Physics Letters*, 166, 275
- Frisch, M. J., Head-Gordon, M., & Pople, J. A. 1990b, *Chemical Physics Letters*, 166, 281
- Frisch, M. J., Trucks, G. W., Schlegel, H. B., et al. 2016, Gaussian-16 Revision C.01, gaussian Inc. Wallingford CT
- Glassgold, A. E. & Langer, W. D. 1974, *ApJ*, 193, 73
- Grimme, S., Antony, J., Ehrlich, S., & Krieg, H. 2010, *The Journal of Chemical Physics*, 132, 154104
- Györffy, W. & Werner, H.-J. 2018, *The Journal of Chemical Physics*, 148, 114104
- Heathcote, D. & Vallance, C. 2018, *Journal of Physics B: Atomic, Molecular and Optical Physics*, 51, 195203
- Helgaker, T., Klopper, W., Koch, H., & Noga, J. 1997, *The Journal of Chemical Physics*, 106, 9639
- Hincelin, U., Wakelam, V., Hersant, F., et al. 2011, *A&A*, 530, A61
- Hindmarsh, A. C. 1983, *IMACS transactions on scientific computation*, 55
- Hwang, W., Kim, Y. K., & Rudd, M. E. 1996, *J. Chem. Phys.*, 104, 2956
- Indriolo, N. & McCall, B. J. 2012, *ApJ*, 745, 91
- Indriolo, N., Neufeld, D. A., Gerin, M., et al. 2015, *ApJ*, 800, 40
- Ivlev, A. V., Padovani, M., Galli, D., & Caselli, P. 2015, *ApJ*, 812, 135
- Ivlev, A. V., Silsbee, K., Padovani, M., & Galli, D. 2021, *ApJ*, 909, 107
- Johnson, Russell D., I. 2022, *NIST Computational Chemistry Comparison and Benchmark Database*, nIST Standard Reference Database Number 101, Release 22
- Kim, Y.-K. & Rudd, M. E. 1994, *Phys. Rev. A*, 50, 3954
- Larsson, M., Geppert, W. D., & Nyman, G. 2012, *Reports on Progress in Physics*, 75, 066901
- Loison, J.-C., Wakelam, V., Hickson, K. M., Bergeat, A., & Mereau, R. 2014, *MNRAS*, 437, 930
- Luo, G., Zhang, Z.-Y., Bisbas, T. G., et al. 2023a, *ApJ*, 942, 101
- Luo, G., Zhang, Z.-Y., Bisbas, T. G., et al. 2023b, *ApJ*, 946, 91
- Marinković, B. P., Jevremović, D., Srećković, V. A., et al. 2017, *European Physical Journal D*, 71, 158
- McElroy, D., Walsh, C., Markwick, A. J., et al. 2013, *A&A*, 550, A36
- Migdal, A. B. & Moszkowski, S. A. 1968, *American Journal of Physics*, 36, 855
- Møller, C. & Plesset, M. S. 1934, *Phys. Rev.*, 46, 618
- Neufeld, D. A., Goicoechea, J. R., Sonnentrucker, P., et al. 2010, *A&A*, 521, L10

¹² <https://github.com/Nicholaswogan/NumbaLSODA>

Neufeld, D. A. & Wolfire, M. G. 2017, *ApJ*, 845, 163

Ortiz, J. V. 2005, *International Journal of Quantum Chemistry*, 105, 803

Padovani, M., Bialy, S., Galli, D., et al. 2022, *A&A*, 658, A189

Padovani, M., Galli, D., & Glassgold, A. E. 2009, *A&A*, 501, 619

Padovani, M., Ivlev, A. V., Galli, D., & Caselli, P. 2018, *A&A*, 614, A111

Phan, V. H. M., Recchia, S., Mertsch, P., & Gabici, S. 2023, *Phys. Rev. D*, 107, 123006

Raghavachari, K., Trucks, G. W., Pople, J. A., & Head-Gordon, M. 1989, *Chemical Physics Letters*, 157, 479

Rivilla, V. M., Sanz-Novo, M., Jiménez-Serra, I., et al. 2023, *ApJ*, 953, L20

Sabatini, G., Bovino, S., Giannetti, A., et al. 2020, *A&A*, 644, A34

Sabatini, G., Bovino, S., & Redaelli, E. 2023, *ApJ*, 947, L18

Shingledecker, C. N., Incerti, S., Ivlev, A., et al. 2020, *ApJ*, 904, 189

Shingledecker, C. N., Lee, K. L. K., Wandishin, J. T., et al. 2021, *A&A*, 652, L12

Silsbee, K. & Ivlev, A. V. 2019, *ApJ*, 879, 14

Sita, M. L., Changala, P. B., Xue, C., et al. 2022, *ApJ*, 938, L12

Smith, D. G. A., Altarawy, D., Burns, L. A., et al. 2020a, *WIREs Computational Molecular Science*, n/a, e1491

Smith, D. G. A., Burns, L. A., Simmonett, A. C., et al. 2020b, *The Journal of Chemical Physics*, 152, 184108

Tielens, A. G. G. M. 2013, *Reviews of Modern Physics*, 85, 1021

Umebayashi, T. & Nakano, T. 1981, *PASJ*, 33, 617

van der Tak, F. F. S. & van Dishoeck, E. F. 2000, *A&A*, 358, L79

van Dishoeck, E. F. 2014, *Faraday Discussions*, 168, 9

Wakelam, V., Herbst, E., Loison, J. C., et al. 2012, *ApJS*, 199, 21

Wakelam, V., Loison, J.-C., Herbst, E., et al. 2015, *The Astrophysical Journal Supplement Series*, 217, 20

Werner, H.-J., Knowles, P. J., Knizia, G., Manby, F. R., & Schütz, M. 2012, *WIREs Comput Mol Sci*, 2, 242

Werner, H.-J., Knowles, P. J., Manby, F. R., et al. 2020, *The Journal of Chemical Physics*, 152, 144107

Yanai, T., Tew, D. P., & Handy, N. C. 2004, *Chemical Physics Letters*, 393, 51

Zhong, L., Wu, B., Zheng, S., & Gu, Q. 2021, *Physics of Plasmas*, 28, 083505

Zhou, W., Wilkinson, L., Lee, J. W. L., Heathcote, D., & Vallance, C. 2019, *Molecular Physics*, 117, 3066

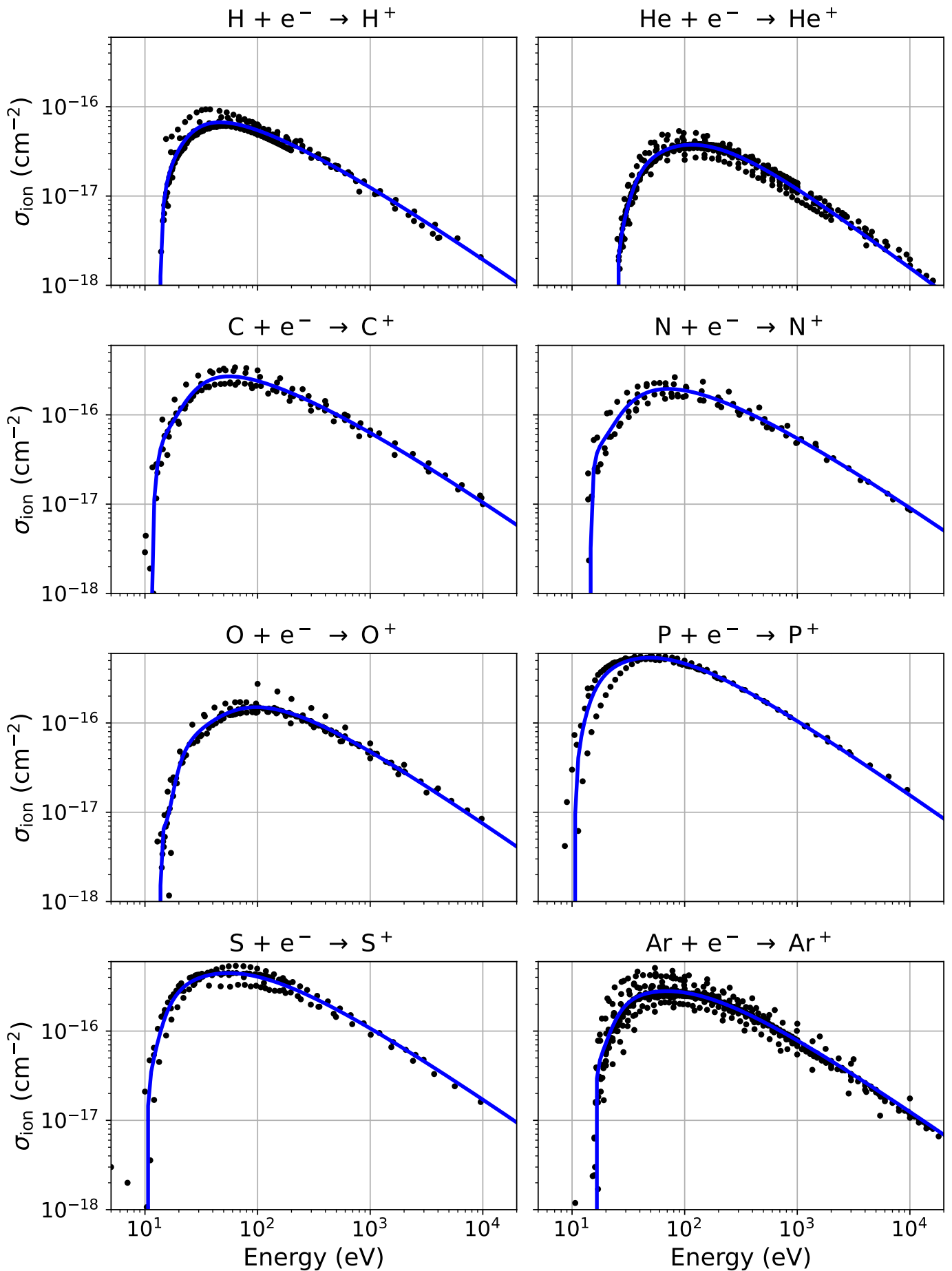


Fig. 1: Electron ionization cross-sections. Solid lines give the fits from Equation 2 and the black points are the data from the NIFS database. Article number, page 9 of ??

Table 3: Unique molecules included (202 total) in this database, sorted by their number of constituent atoms.

Atoms	2 atoms	3 atoms	4 atoms	5 atoms	6 atoms	7 atoms	8 atoms	9 atoms	10-15 atoms	15+ atoms
H	C ₂	C ₂ H	C ₂ H ₂ O	C ₂ H ₄	C ₂ H ₄ O	C ₂ H ₃ NH ₂	C ₂ H ₅ CN	C ₁₀ H ₂	C ₁₄ H ₁₀	
He	CF ⁺	C ₃	C ₂ N ₂	C ₂ H ₃	C ₃ H ₃	C ₂ H ₅	C ₂ H ₅ OH	C ₂ H ₅ CHO	C ₅ H ₁₀	
Ar	CH ⁺	CCN	C ₃ H	C ₂ HNO	C ₅ H	C ₆ H	C ₃ H ₅	C ₂ H ₅ OCH ₃	C ₅ H ₁₁	
C	CN	CCO	C ₃ H ⁺	C ₃ H ₂	CH ₂ CCO	CH ₂ CHCN	C ₄ H ₄	C ₅ H ₅	C ₅ H ₁₂	
N	CO	CH ₂	C ₃ N	C ₄ H	CH ₂ NH ₂	CH ₃ C ₂ H	C ₇ H	C ₅ H ₄	C ₆ H ₁₀	
O	CO ⁺	CO ₂	C ₃ O	C ₅	CH ₂ NH	CH ₃ CN	CH ₂ CHCHO	C ₈ H	C ₆ H ₁₁	
S	CS	CP	H ₂ O	C ₄	CH ₂ OH	CH ₃ NC	CH ₃ C ₃ N	C ₃ H ₈	C ₆ H ₁₂	
P	H ₂ O ⁺	H ₂ O	CH ₃	CH ₂ PH	CH ₃ NH	CH ₃ CHS	CH ₃ COCN	C ₄ H ₁₀	C ₆ H ₁₃	
	H ₂	H ₂ S	CHNO	CH ₂ SH	CH ₃ NCO	CH ₃ OC ₂ H ₂	CH ₃ CONH ₂	C ₄ H ₇	C ₆ H ₁₄	
	HF	H ₃ ⁺	CO ₂ H ⁺	CO ₂ H ₂	CH ₃ OH	CH ₃ OH	HC ₆ H	C ₄ H ₈	C ₆ H ₉	
	HS	HCN	H ₂ CN	H ₂ C ₃ O	CH ₃ O	CH ₃ NH ₂	HCOOCH ₃	C ₅ H ₅	C ₇ H ₁₀	
	N ₂	HCO	H ₂ CS	H ₂ CCN	H ₂ CCNH	H ₂ CCHOH	NC ₆ N	C ₅ H ₆	C ₇ H ₈	
	NH	HCO ⁺	H ₂ O ₂	H ₂ CCN	H ₂ CCS	HC ₂ CHO	NH ₂ CH ₂ CN	C ₅ H ₇	C ₆ H ₇	
	NO	HNC	H ₃ O ⁺	H ₂ O ₂	H ₂ NC ⁺	HC ₃ NH ⁺	HC ₃ NH ₂	C ₅ H ₈	C ₆ H ₈	
	NO ⁺	HNO	HO ₂	HCCN	HC ₂ NC	HC ₄ H	HC ₄ N	C ₅ H ₉	C ₆ H ₉	
	NS	HO ₂	HOC ⁺	HCN ⁺	HC ₃ N	HCOCHO	HNCHCN	C ₆ H ₅ CN	C ₆ H ₄	
	O ₂	OH	HPO	HCNO	HC ₃ O	HNCHSH	N ₂ H ₄	C ₆ H ₆	C ₆ H ₇	
	OH ⁺	N ₂ H ⁺	HCNS	HCCO	HCNCC	NC ₄ N	NC ₄ N	C ₆ H ₈	C ₇ H ₄	
	PH	N ₂ O	HNCO	HCOOH	NH ₂ CHO	NH ₂ CHS	NH ₂ CHS	C ₇ H ₇	C ₇ H ₇	
	PN	NH ₂	HNCS	HOOC	NHC ₃	NCCNH ⁺	NCCNH ⁺	C ₈ H ₂	C ₈ H ₆	
	PO	NO ₂	O ₃	HSCN	N ₂ H ₃	NH ₂ CN	NH ₂ CN	CH ₂ CHCHCH ₂	CH ₂ OHCH ₂ OH	
	S ₂	OCN	OCN	HSSH	N ₂ H ₃	NH ₄ ⁺	NH ₄ ⁺	CH ₃ C ₅ N	CH ₃ C ₆ H	
	SO	PH ₂	SO ₂	NO ₃	NO ₃	NO ₃	SO ₃	CH ₃ COOCH ₃	CH ₃ COOCH ₂ OH	
								HC ₁₁ N	HC ₉ N	
								HCOOC ₂ H ₅		

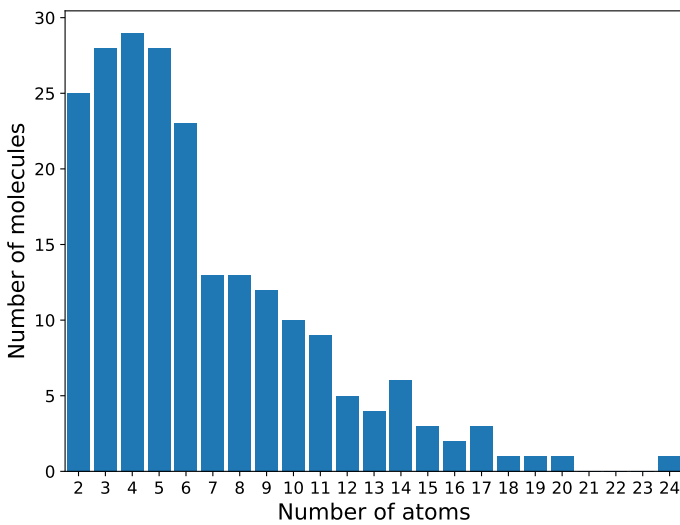


Fig. 2: Distribution of the number of atoms in each molecule for this data release.

Table 5: Molecular orbitals of CO, computed at the MP2/aug-cc-pVTZ level. All energies are in eV. The orbital kinetic energy (KE), the orbital binding energy based on canonical HF orbitals (BE-HF), the orbital binding energy based on EPT computation (BE-EPT) and the corresponding pole strength (PS) are displayed. *** denote no data, since EPT energies for pole strengths less than 0.8 (electrons deep within the potential) are not considered.

Orbital number	KE	BE-HF	BE-EPT	PS
1	794.32671	562.41699	***	***
2	436.29414	309.24685	***	***
3	78.26264	41.33263	***	***
4	71.85773	21.8887	***	***
5	53.94510	17.35920	17.015	0.903
6	53.94510	17.35920	17.015	0.903
7	42.78816	15.11922	14.266	0.910

Table 6: Same as Table 5 but for H₂O.

Orbital number	KE	BE-HF	BE-EPT	PS
1	794.31517	559.67367	***	***
2	71.17519	36.81820	***	***
3	48.69143	19.49103	18.872	0.933
4	58.43876	15.92808	14.802	0.925
5	60.77375	13.88698	12.554	0.921

Table 8: Initial abundances as a function of the total H nuclei abundance, i.e. $n_{\text{H},\text{tot}}$ (Hincelin et al. 2011). We assume $a(b) = a \times 10^b$.

Species	Abundance	Species	Abundance
H ₂	5(-1)	P	2(-10)
He	9(-2)	N	6.2(-5)
C	1.7(-4)	O	2.4(-4)
S	8(-8)	Si	8(-9)
Fe	3(-9)	Na	2(-9)
Mg	7(-9)	Cl	1(-9)

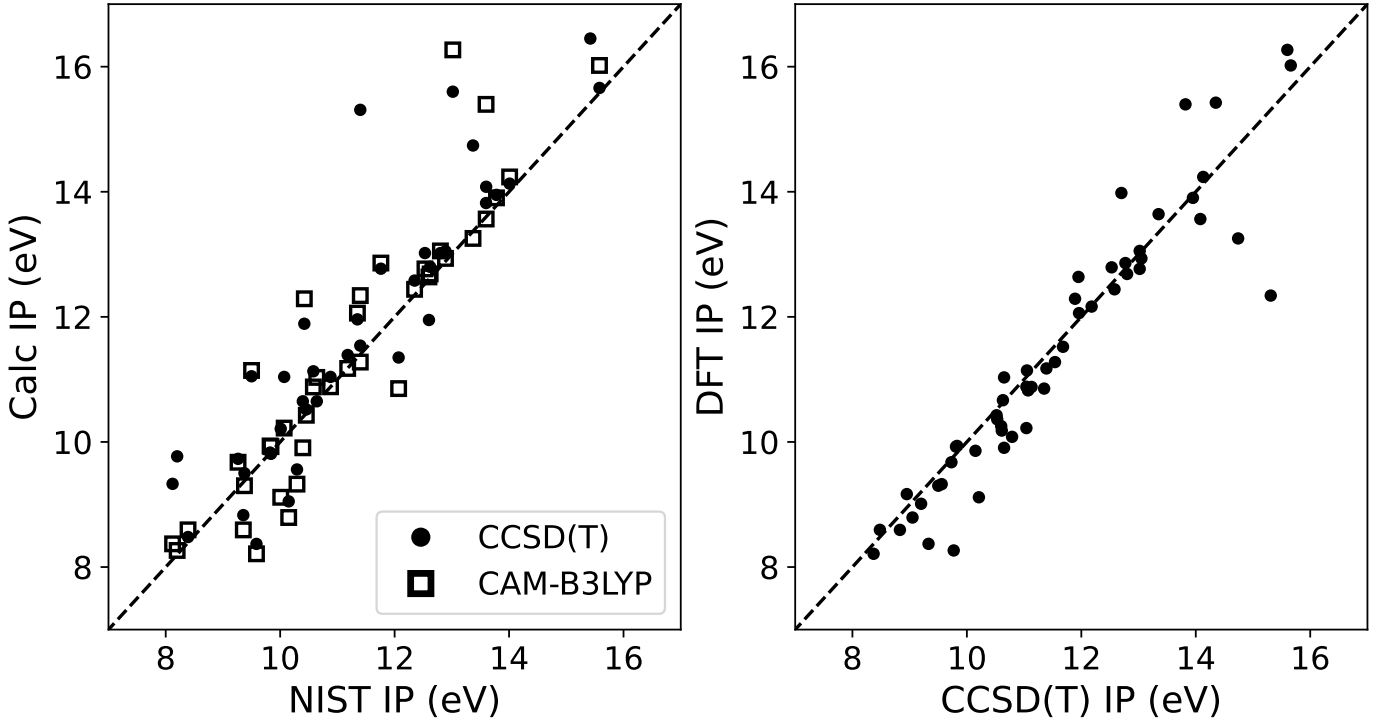


Fig. 3: Comparison of ionization potentials presented here against the NIST database. Left: NIST database vs CCSD(T) and CAM-B3LYP DFT calculations (solid and empty square, respectively). Right: CCSD(T) vs CAM-B3LYP DFT ionization potentials. The dashed line represents the one-to-one ratio.

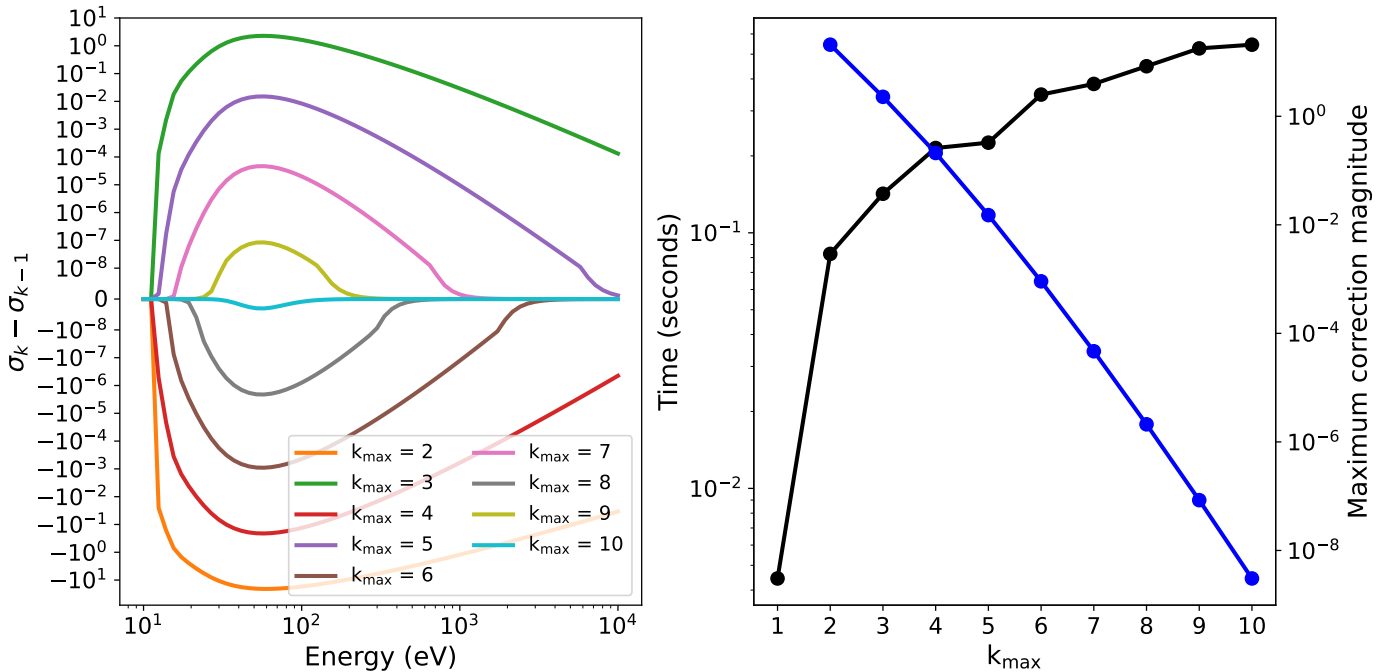


Fig. 4: Left: k -atom screening corrections as a function of electron energy for C_5H_{10} . Right: Time to compute $\sigma_{\text{SCAR}}(E_e)$ for a given maximum k -atom screening correction (black) and the magnitude of the maximal correction (blue) as a function of the maximum k .

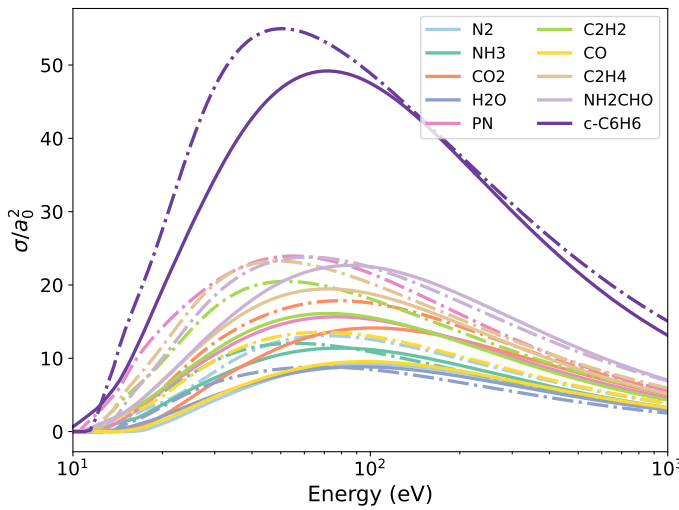


Fig. 5: Sample of the total electron ionization cross-sections for a sub-sample of the molecules. Solid denotes cross-sections calculated using the BEB method, and the dotted line uses the SCAR rule.

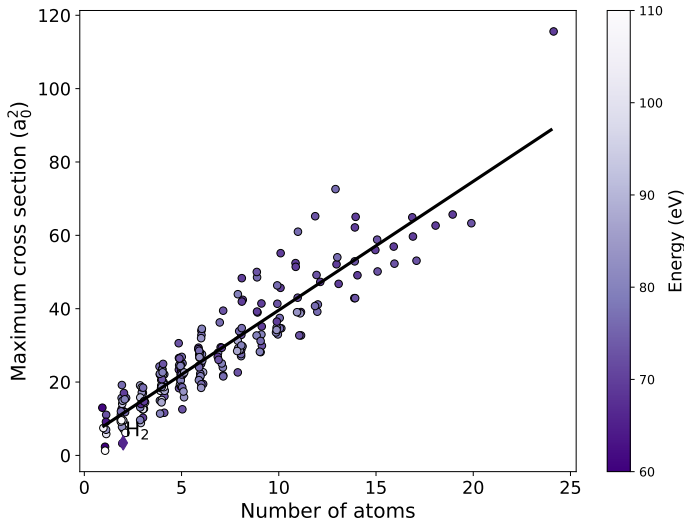


Fig. 6: Maximum of the electron-impact ionization cross-section as a function of the number of atoms in a molecule. The color denotes the electron energy in eV the maximum occurs.

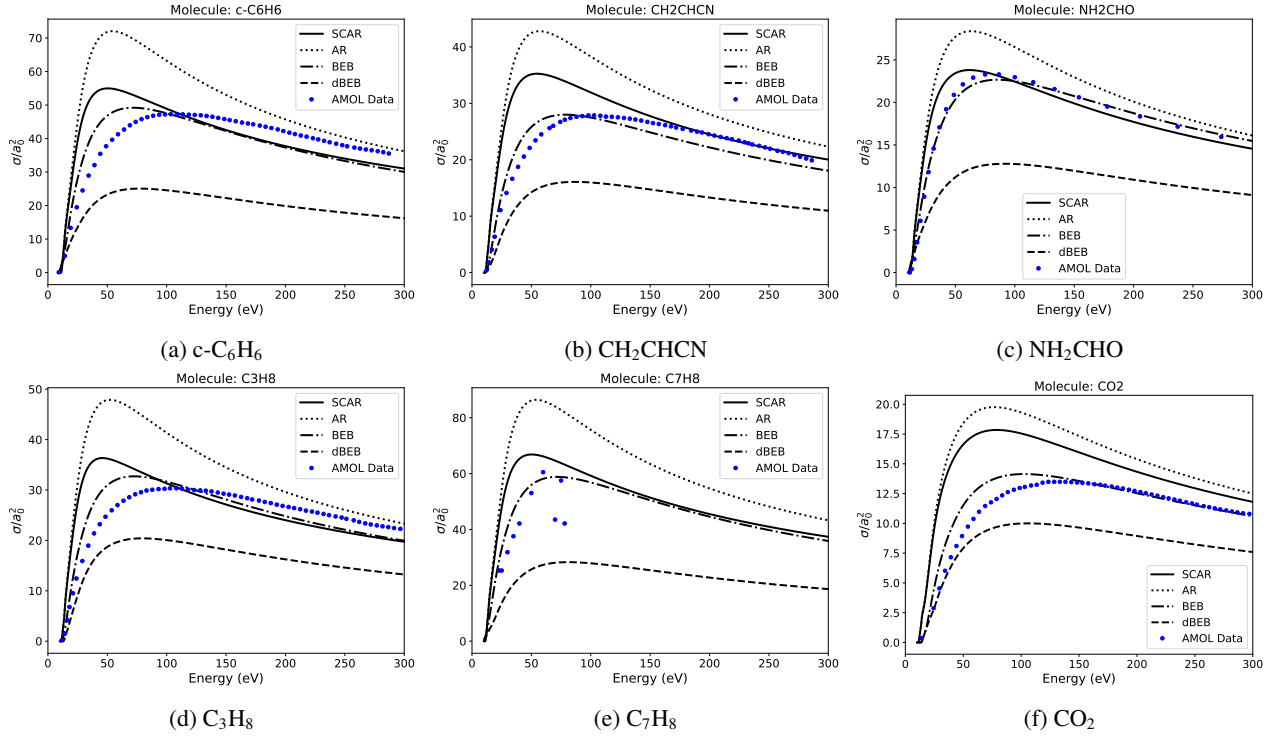


Fig. 7: Electron ionization cross-sections computed with the IAM-AR (dashed), SCAR (solid), and BEB (dashed-dotted) methods compared against experimental data from the NIFS database (blue dots).

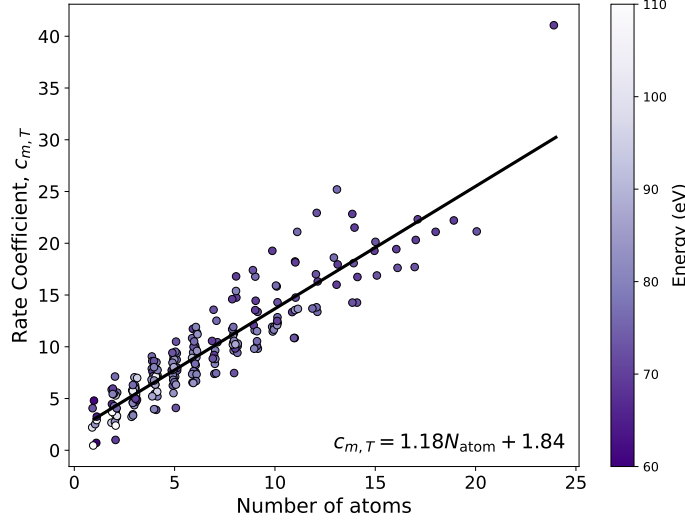


Fig. 8: Total ionization rate coefficient, $C_{m,T}$, as a function of the constituent number of atoms in each molecule. The color denotes the energy at the cross-section maximum.

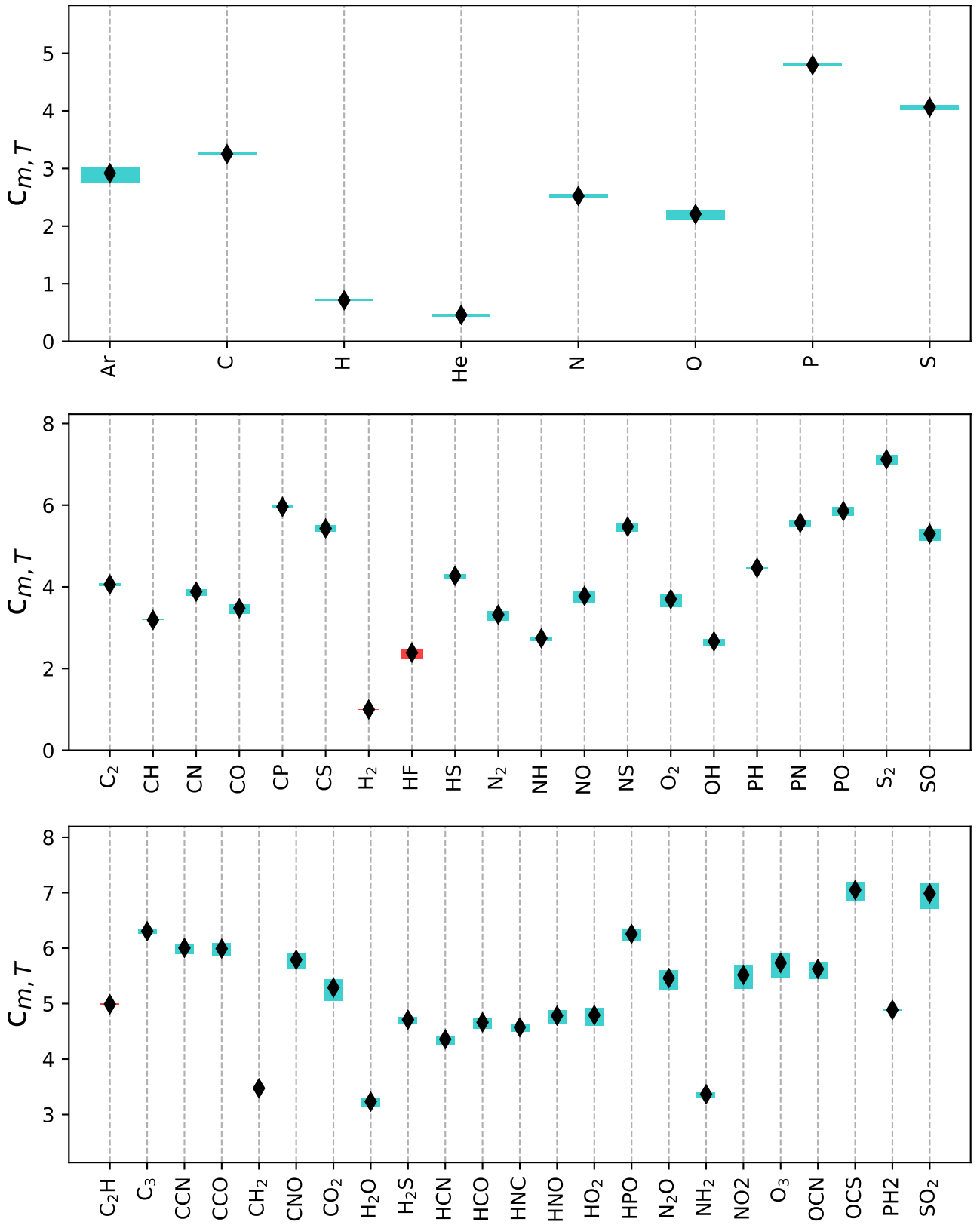


Fig. 9: Reaction rate coefficients, following Equation 13 for all neutral molecules in the database. The boxes show the minimum and maximum coefficients in the column density range $10^{20} \text{ cm}^{-2} \leq N_{\text{H}_2} \leq 10^{23} \text{ cm}^{-2}$, plus signs show the mean. The cyan boxes denote molecules using MP2 calculations while red denote calculations from [Heathcote & Vallance \(2018\)](#).

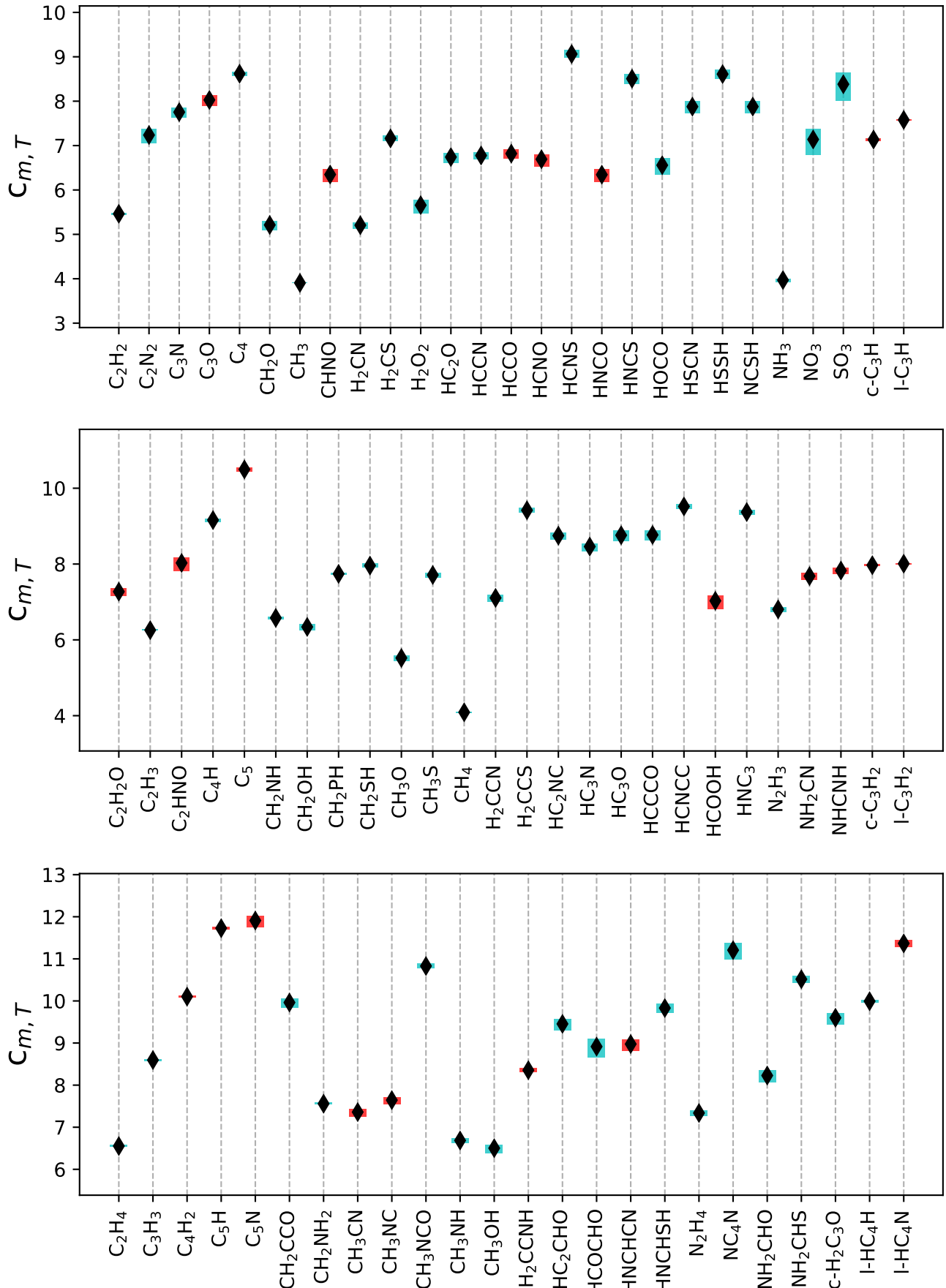


Fig. 10: Figure 9 cont.

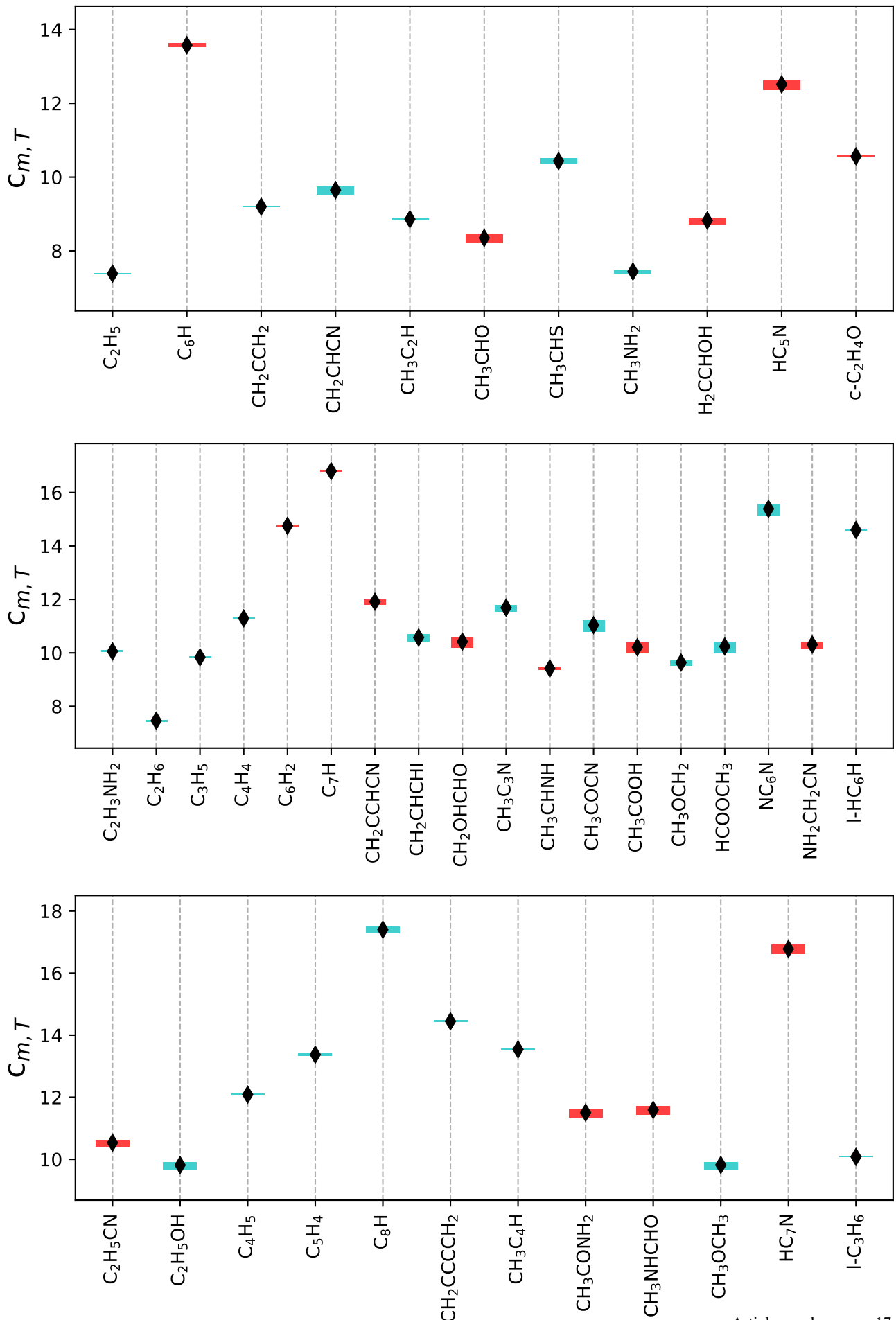


Fig. 11: Figure 10 cont.

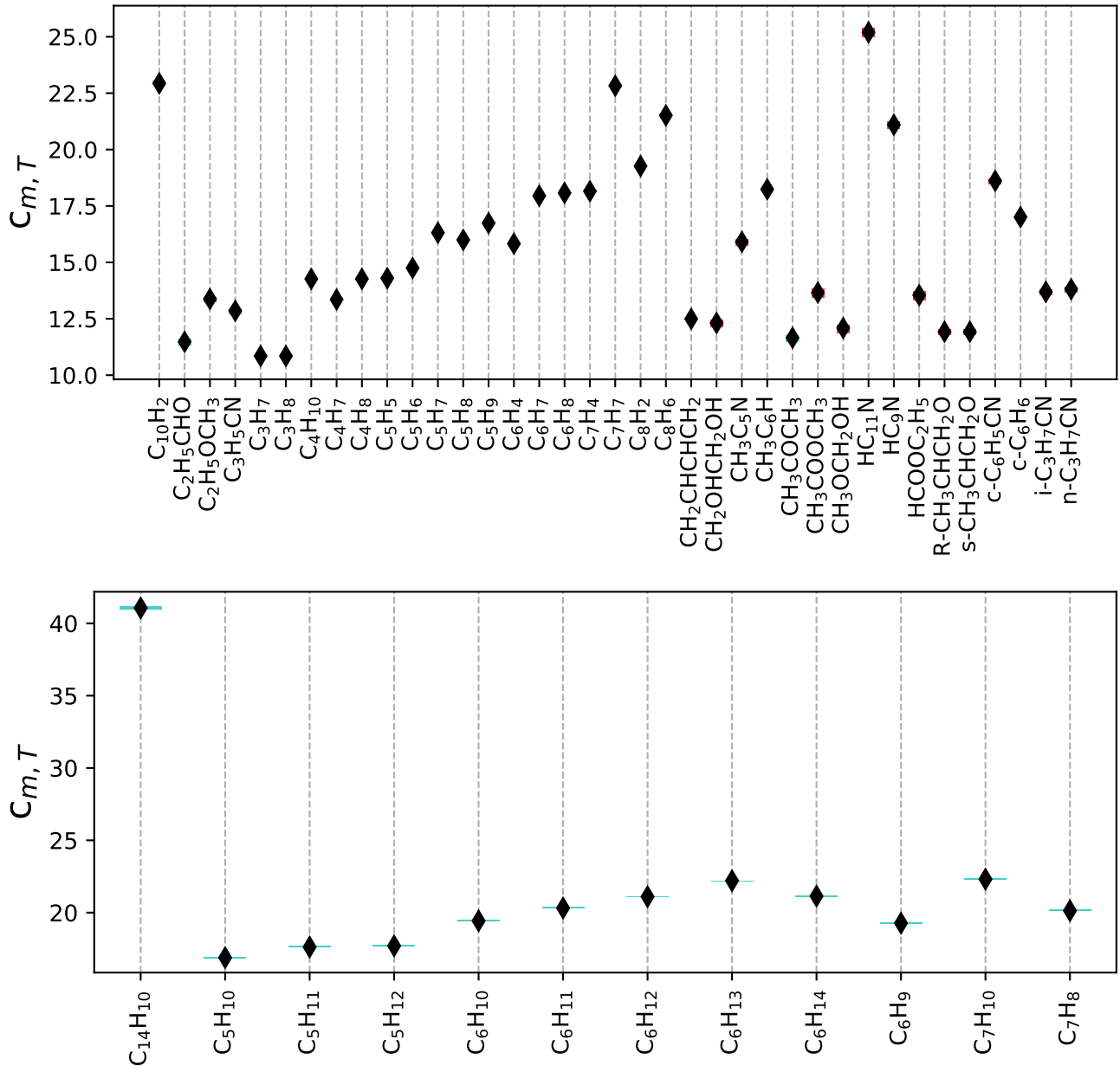


Fig. 12: Figure 11 cont.

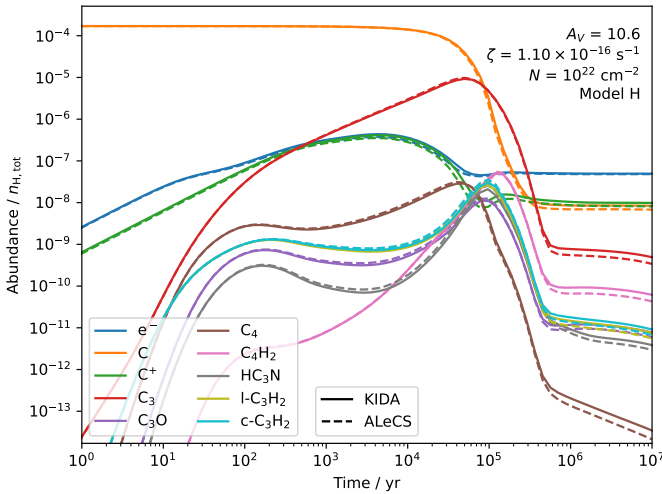


Fig. 13: Comparison of the chemical evolution using KIDA reaction rates (solid lines) and ours (dashed lines). We report the species that present a difference of at least half an order of magnitude and reach at least $n(t) = 10^{-8}n_{H,\text{tot}}$. The ionization rate of H_2 is $1.64 \times 10^{-16} \text{ s}^{-1}$, that for model ‘High’ and with the assumptions described in the text, corresponds to $A_V=10.6$ and $N=10^{22} \text{ cm}^{-2}$.

Table 4: Ionization potentials in eV, computed at the CCSD(T)/CBS, CAM-B3LYP/aug-cc-pVQZ and from NIST.

Molecule	IP (CCSD(T))	IP (DFT)	IP ¹³ (NIST)
Diatom	IP (CCSD(T))	IP (DFT)	IP (NIST)
C ₂	15.31	12.34	11.40
CH	10.65	11.03	10.64
CN	13.82	15.40	13.60
CO	14.13	14.24	14.01
CP		11.79	
CS		11.45	
H ₂	16.45		15.42
HS	11.89	12.29	10.42
N ₂	15.66	16.02	15.58
NH	11.68	11.52	
NO	9.73	9.68	9.26
NS	8.95	9.17	
O ₂	11.35	10.85	12.07
OH	15.60	16.27	13.02
PH	9.05	8.79	10.15
PN		11.89	
PO	8.48	8.59	8.39
S ₂	8.83	8.59	9.36
SO	9.56	9.33	10.29
Triatomic	IP (CCSD(T))	IP (DFT)	IP (NIST)
C ₃	11.95	12.64	12.60
CCN		11.21	
CCO	10.60	10.25	
CH ₂	10.65	9.91	10.40
CNO	12.77	12.86	11.76
CO ₂	13.95	13.90	13.78
H ₂ O	12.80	12.69	12.62
H ₂ S	10.52	10.43	10.46
HCN	14.08	13.56	13.60
HCO	9.33	8.37	8.12
HNC	12.18	12.16	
HNO	10.61	10.18	
HPO	10.53	10.36	
N ₂ O	13.05	12.93	12.89
NH ₂	12.53	12.79	
NO ₂	8.37	8.21	9.59
O ₂ H	11.96	12.06	11.35
O ₃	13.02	12.77	12.53
OCN	13.35	13.64	
OCS	11.39	11.18	11.18
PH ₂	9.83	9.94	9.82
SO ₂	12.58	12.44	12.35
4-atomic	IP (CCSD(T))	IP (DFT)	IP (NIST)
C ₂ H ₂	11.54	11.28	11.40
C ₂ N ₂	14.74	13.25	13.37
C ₃ N	14.35	15.42	
C ₄		10.56	
CH ₃	9.81	9.92	9.84

Table 4: continued.

Molecule	IP (CCSD(T))	IP (DFT)	IP (NIST)
H ₂ C ₃ O		10.59	
H ₂ CN	10.63	10.67	
H ₂ CO	11.04	10.88	10.88
H ₂ CS	9.50	9.30	9.38
HC ₂ N	10.79	10.08	
HC ₂ O	11.05	11.14	9.50
HCNS	9.20	9.01	
HNCS	10.15	9.86	
HOCO	9.77	8.27	8.20
HOOH	11.13	10.88	10.58
HSCN	11.07	10.83	
HSSH	10.21	9.12	10.01
NCSH	11.07	10.83	
NH ₃	11.04	10.22	10.07
NO ₃	12.70	13.98	
SO ₃	13.02	13.05	12.80
5-atomic	IP (CCSD(T))	IP (DFT)	IP (NIST)
C ₂ H ₃		8.73	
C ₂ H ₃ CHO		9.99	
C ₄ H		14.39	
CH ₂ NH		9.92	
CH ₂ OH		7.62	
CH ₂ PH		10.04	
CH ₂ SH		7.63	
CH ₃ O		8.89	
CH ₃ S		10.24	
CH ₄		12.72	
H ₂ CCN		10.42	
H ₂ CCS		8.86	
HC ₃ N		11.48	
HC ₃ O		11.26	
HCCCO		7.57	
HCCNC		11.04	
HCNCC		11.09	
N ₂ H ₃		7.81	
6-atomic	IP (CCSD(T))	IP (DFT)	IP (NIST)
C ₂ H ₄		10.40	
C ₃ H ₃		8.76	
CH ₂ CCO		9.02	
CH ₂ NH ₂		6.28	
CH ₃ NCO		9.59	
CH ₃ NH		15.09	
CH ₃ OH		10.80	
HCOCHO		10.16	
HNCHSH		9.71	
N ₂ H ₄		6.82	
NC ₄ N		11.67	
NH ₂ CHO		10.13	
NH ₂ CHS		8.54	

Table 4: continued.

Molecule	IP (CCSD(T))	IP (DFT)	IP (NIST)
c-H ₂ C ₃ O		9.45	
l-HC ₄ H		9.96	
7-atomic	IP (CCSD(T))	IP (DFT)	IP (NIST)
C ₂ H ₅		8.19	
CH ₂ CCH ₂		7.24	
CH ₂ CHCN		10.72	
CH ₃ CHS		8.85	
CH ₃ NH ₂		9.00	
8-atomic	IP (CCSD(T))	IP (DFT)	IP (NIST)
C ₂ H ₃ NH ₂		7.98	
C ₂ H ₆		11.59	
C ₃ H ₅		7.77	
C ₄ H ₄		9.32	
CH ₃ C ₃ N		10.59	
CH ₃ COCN		11.16	
CH ₃ OCH ₂		7.05	
HCOOCH ₃		10.74	
HNCCC		9.80	
NC ₆ N		10.69	
l-HC ₆ H		9.26	
9-atomic	IP (CCSD(T))	IP (DFT)	IP (NIST)
C ₄ H ₅		7.96	
C ₅ H ₄		10.03	
C ₈ H		8.81	
CH ₂ CCCCH ₂		8.55	
CH ₃ C ₄ H		9.26	
CH ₃ OCH ₃		9.85	
l-C ₃ H ₆		9.57	
10-atomic and more	IP (CCSD(T))	IP (DFT)	IP (NIST)
C ₁₀ H ₂		8.50	
C ₂ H ₅ CHO		9.92	
C ₃ H ₅ CN		10.00	
C ₃ H ₇		10.99	
C ₃ H ₈		10.99	
C ₄ H ₁₀		10.89	
C ₄ H ₇		7.58	
C ₄ H ₈		10.89	
C ₅ H ₅		7.80	
C ₅ H ₆		8.74	
C ₅ H ₇		7.42	
C ₅ H ₈		8.35	
C ₆ H ₄		8.74	
C ₆ H ₇		7.31	
C ₆ H ₈		8.70	
C ₇ H ₄		7.98	
C ₈ H ₂		8.81	
C ₈ H ₆		8.65	
CH ₂ CHCHCH ₂		8.80	
CH ₃ C ₆ H		8.73	

Table 4: continued.

Molecule	IP (CCSD(T))	IP (DFT)	IP (NIST)
CH ₃ CCH		10.21	
CH ₃ CH ₂ OH		10.38	
CH ₃ COCH ₃		9.64	
c-C ₆ H ₆		9.17	
C ₁₄ H ₁₀		7.21	
C ₅ H ₁₂		10.76	
C ₆ H ₁₀		8.27	
C ₆ H ₁₂		9.29	
C ₆ H ₁₄		10.77	
C ₆ H ₉		6.97	
C ₇ H ₈		9.09	

Table 7: Table of the chemical reaction rates, $c_{m,T}$

Atom	$c_{m,T}$
H	0.713
He	0.459
C	3.252
N	2.522
O	2.208
P	4.796
S	4.064
Ar	2.919
Diatom	$c_{m,T}$
<chem>C2</chem>	4.061
<chem>CF+</chem>	1.383
<chem>CH</chem>	3.190
<chem>CH+</chem>	0.795
<chem>CN</chem>	3.881
<chem>CN-</chem>	28.653
<chem>CO</chem>	3.476
<chem>CO+</chem>	1.401
<chem>CP</chem>	5.960
<chem>CS</chem>	5.432
<chem>H2</chem>	1.000
<chem>HF</chem>	2.388
<chem>HS</chem>	4.271
<chem>N2</chem>	3.319
<chem>NH</chem>	2.740
<chem>NO</chem>	3.779
<chem>NO+</chem>	1.316
<chem>NS</chem>	5.474
<chem>O2</chem>	3.699
<chem>OH</chem>	2.666
<chem>OH+</chem>	0.809
<chem>PH</chem>	4.465
<chem>PN</chem>	5.570
<chem>PO</chem>	5.855
<chem>S2</chem>	7.123
<chem>SO</chem>	5.300
Triatomic	$c_{m,T}$
<chem>C2H</chem>	4.987
<chem>C3</chem>	6.306
<chem>CCN</chem>	6.004
<chem>CCO</chem>	5.990
<chem>CH2</chem>	3.473
<chem>CNO</chem>	5.790
<chem>CO2</chem>	5.287
<chem>H2O</chem>	3.232
<chem>H2O+</chem>	1.028
<chem>H2S</chem>	4.710
<chem>H3+</chem>	0.306
<chem>HCN</chem>	4.357
<chem>HCO</chem>	4.662
<chem>HCO+</chem>	1.643

Table 7: continued.

Molecule	$c_{m,T}$
HNC	4.574
HNO	4.783
HO ₂	4.792
HOC ⁺	1.705
HPO	6.258
N ₂ H ⁺	1.622
N ₂ O	5.460
NH ₂	3.366
NO ₂	5.517
O ₃	5.734
OCN	5.625
OCS	7.049
PH ₂	4.887
SO ₂	6.986
4-atomic	$c_{m,T}$
C ₂ H ₂	5.463
C ₂ N ₂	7.237
C ₃ N	7.753
C ₃ N ⁺	35.329
C ₃ O	8.028
C ₄	8.618
CH ₂ O	5.212
CH ₃	3.906
CHNO	6.348
CO ₂ H ⁺	2.713
H ₂ CN	5.206
H ₂ CS	7.162
H ₂ O ₂	5.657
H ₃ O ⁺	1.281
HC ₂ O	6.741
HCCN	6.777
HCCO	6.820
HCNH ⁺	1.924
HCNO	6.692
HCNS	9.062
HNCO	6.345
HNCS	8.507
HOCO	6.558
HSCN	7.877
HSSH	8.610
NCSH	7.878
NH ₃	3.971
NO ₃	7.138
SO ₃	8.382
c-C ₃ H	7.137
l-C ₃ H	7.579
l-C ₃ H ⁺	2.881
5-atomic	$c_{m,T}$
C ₂ H ₂ O	7.272
C ₂ H ₃	6.257

Table 7: continued.

Molecule	$c_{m,T}$
C ₂ HNO	8.029
C ₄ H	9.160
C ₄ H ⁺	47.898
C ₅	10.496
CH ₂ NH	6.580
CH ₂ OH	6.342
CH ₂ PH	7.740
CH ₂ SH	7.959
CH ₃ O	5.522
CH ₃ S	7.711
CH ₄	4.090
H ₂ CCN	7.107
H ₂ CCS	9.419
H ₂ NCO ⁺	4.804
HC ₂ NC	8.750
HC ₃ N	8.461
HC ₃ O	8.760
HCCCO	8.768
HCNCC	9.519
HCOOH	7.030
HNC ₃	9.371
N ₂ H ₃	6.805
NCCNH ⁺	3.890
NH ₂ CN	7.681
NH ₄ ⁺	1.469
NHCNH	7.828
c-C ₃ H ₂	7.969
l-C ₃ H ₂	8.009
<hr/>	
6-atomic	$c_{m,T}$
C ₂ H ₄	6.552
C ₃ H ₃	8.596
C ₄ H ₂	10.103
C ₅ H	11.728
C ₅ N	11.910
C ₅ N ⁺	41.216
CH ₂ CCO	9.963
CH ₂ NH ₂	7.559
CH ₃ CN	7.360
CH ₃ NC	7.644
CH ₃ NCO	10.829
CH ₃ NH	6.685
CH ₃ OH	6.502
H ₂ CCNH	8.355
HC ₂ CHO	9.454
HC ₃ NH ⁺	4.418
HCOCHO	8.916
HNCHCN	8.976
HNCHSH	9.831
N ₂ H ₄	7.337
NC ₄ N	11.206

Table 7: continued.

Molecule	$c_{m,T}$
NH ₂ CHO	8.228
NH ₂ CHS	10.516
c-H ₂ C ₃ O	9.600
l-HC ₄ H	9.993
l-HC ₄ N	11.367
7-atomic	$c_{m,T}$
C ₂ H ₅	7.383
C ₆ H	13.576
C ₆ H ⁺	50.847
CH ₂ CCH ₂	9.199
CH ₂ CHCN	9.646
CH ₃ C ₂ H	8.860
CH ₃ CHO	8.352
CH ₃ CHS	10.436
CH ₃ NH ₂	7.440
H ₂ CCHOH	8.824
HC ₅ N	12.515
c-C ₂ H ₄ O	10.563
8-atomic	$c_{m,T}$
C ₂ H ₃ NH ₂	10.056
C ₂ H ₆	7.462
C ₃ H ₅	9.836
C ₄ H ₄	11.289
C ₆ H ₂	14.753
C ₇ H	16.800
CH ₂ CCHCN	11.912
CH ₂ CHCHO	10.575
CH ₂ OHCHO	10.422
CH ₃ C ₃ N	11.691
CH ₃ CHNH	9.417
CH ₃ COCN	11.037
CH ₃ COOH	10.210
CH ₃ OCH ₂	9.636
HCOOCH ₃	10.238
NC ₆ N	15.387
NH ₂ CH ₂ CN	10.308
l-HC ₆ H	14.597
9-atomic	$c_{m,T}$
C ₂ H ₅ CN	10.534
C ₂ H ₅ OH	9.813
C ₄ H ₅	12.083
C ₅ H ₄	13.373
C ₈ H	17.401
C ₈ H ⁺	54.738
CH ₂ CCCCH ₂	14.448
CH ₃ C ₄ H	13.542
CH ₃ CONH ₂	11.505
CH ₃ NHCHO	11.590
CH ₃ OCH ₃	9.817
HC ₇ N	16.778

Table 7: continued.

Molecule	$c_{m,T}$
l-C ₃ H ₆	10.079
10-atomic and more	$c_{m,T}$
C ₁₀ H ₂	22.934
C ₂ H ₅ CHO	11.476
C ₂ H ₅ OCH ₃	13.377
C ₃ H ₅ CN	12.852
C ₃ H ₇	10.849
C ₃ H ₈	10.849
C ₄ H ₁₀	14.267
C ₄ H ₇	13.353
C ₄ H ₈	14.267
C ₅ H ₅	14.297
C ₅ H ₆	14.750
C ₅ H ₇	16.314
C ₅ H ₈	15.996
C ₅ H ₉	16.741
C ₆ H ₄	15.829
C ₆ H ₇	17.953
C ₆ H ₈	18.079
C ₇ H ₄	18.154
C ₇ H ₇	22.830
C ₈ H ₂	19.269
C ₈ H ₆	21.514
CH ₂ CHCHCH ₂	12.495
CH ₂ OHCH ₂ OH	12.313
CH ₃ C ₅ N	15.909
CH ₃ C ₆ H	18.239
CH ₃ COCH ₃	11.656
CH ₃ COOCH ₃	13.661
CH ₃ OCH ₂ OH	12.089
HC ₁₁ N	25.198
HC ₉ N	21.100
HCOOC ₂ H ₅	13.549
R-CH ₃ CHCH ₂ O	11.925
S-CH ₃ CHCH ₂ O	11.925
c-C ₆ H ₅ CN	18.613
c-C ₆ H ₆	17.007
i-C ₃ H ₇ CN	13.695
n-C ₃ H ₇ CN	13.813
C ₁₄ H ₁₀	41.065
C ₅ H ₁₀	16.887
C ₅ H ₁₁	17.624
C ₅ H ₁₂	17.702
C ₆ H ₁₀	19.434
C ₆ H ₁₁	20.318
C ₆ H ₁₂	21.104
C ₆ H ₁₃	22.204
C ₆ H ₁₄	21.143
C ₆ H ₉	19.272
C ₇ H ₁₀	22.314

Table 7: continued.

Molecule	$c_{m,T}$
C ₇ H ₈	20.136